NMR Study of Some Thermotropic Nematic Polyesters with Mesogenic Elements and Flexible Spacers in the Main Chain

Assis F. Martins* and Jorge B. Ferreira

Centro de Física da Matéria Condensada, INIC, 2, Av. Prof. Gama Pinto, 1699 Lisboa Codex, Portugal

Ferdinand Volino

CNRS et Equipe de Physico-Chimie Moléculaire, SPS/DRF, CENG, 85X, 38041 Grenoble Cedex, France

Alexandre Blumstein and Rita B. Blumstein

Department of Chemistry, Polymer Program, University of Lowell, Lowell, Massachusetts 01854. *Received April 8, 1982*

ABSTRACT: We report the results of a proton NMR investigation of a new class of thermotropic nematic liquid crystalline polyesters with mesogenic elements and flexible spacers in the main chain. The NMR line shapes and line widths as a function of temperature are used to derive information on the molecular organization and dynamics in the solid and nematic phases of samples differing by their molecular weight and spacer length. Homogeneous orientation of the macromolecules in the nematic phase was observed for a sample of $\bar{M}_n \simeq 4000$ in the magnetic field of 11.7 kG used in the NMR experiment. The nematic order parameter of this sample was found to vary between 0.69 at the nematic–isotropic and 0.84 at the solid–nematic transition temperature, thus taking unusually high values. From a detailed analysis of the corresponding NMR spectrum we show that the flexible spacers align in the magnetic field with a degree of order comparable to that of the mesogenic elements, which implies that the macromolecules take, on the average, a rather extended conformation.

1. Introduction

Spurred by the search for ultrahigh-strength fibers, investigations in the field of liquid crystalline polymers have come to the forefront of industrial and academic research. Current work is focused primarily on linear polymers in which the mesogenic elements are incorporated into the main chain. The mesogenic moieties, which are not always mesomorphic in their own right, can induce mesomorphic behavior in the polymer either upon heating (thermotropic liquid crystals) or through solvation (lyotropic liquid crystals).

Perhaps the best known systems at this time are the high-modulus fibers spun from lyotropic nematic solutions of polyaramides[1,2] or from thermotropic melts of *p*-oxybenzoate-modified poly(ethylene terephthalate).[3,4] The phase transition temperatures of these systems tend to be very high and thermal degradation often occurs before the onset of melting or clearing.

On the other hand, polymers in which the mesogenic elements are separated by flexible spacer groups such as $-[CH_2]-_n$, $-[CH_2CH_2O]-_n$, or $-[Si(CH_3)_2O]-_n$, can give thermotropic mesophases in which the transition temperatures are well below the range of thermal degradation of the macromolecule. A variety of smectic, nematic,[5-13] and, recently, cholesteric[14-17] polymers have been prepared, typically by condensation of mesogenic diols, diphenols, or diacid chlorides with flexible diols or diacid chlorides.

In this paper we report the results of a proton NMR investigation of two novel, low-melting nematic polymers prepared by condensation of 2,2′-dimethyl-4,4′-azoxybenzene with the diacid chloride of dodecanedioic or 3-methyladipic acid. The corresponding polymers, labeled DDA9 and MAA9, respectively, have the structural formulas

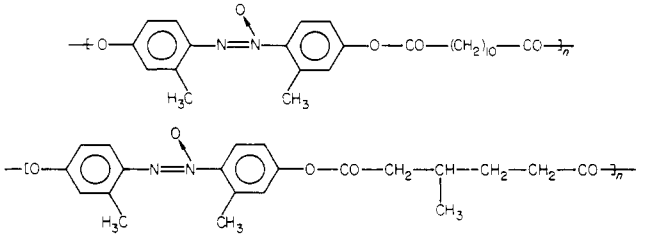

Table I
Physical Characteristics of Samples Investigated

sample	$\bar{M}_n$	$\bar{DP}$	T_{KN}, °C	T_{NI}, °C
DDA9-L	4 000	9	99	135.5
DDA9-H	20 000	42	119	165
MAA9-H	16 000	42	169	231

The mesogenic moiety of these polymers contains an azoxy functional group and differs from the extensively investigated nematic *p*-azoxyanisole (PAA) only by the presence of a methyl group in the 2 and 2′ positions.

The symbols used to represent the samples that we have investigated, their number-average molecular weight ($\bar{M}_n$), and average degree of polymerization ($\bar{DP}$) are listed in Table I together with T_{KN} and T_{NI}, the solid-to-nematic and nematic-to-isotropic transition temperatures. It is noteworthy that the nematic temperature range of these polymers is wider than in the case of PAA, which displays a nematic phase between 118.2 and 135.3 °C. Table I also shows the influence of spacer length on phase transition temperatures as well as the influence of molecular weight on the transition temperatures and nematic range of DDA9 samples.

The remainder of this paper is organized as follows. In section 2 we point out the techniques used in this work and report our main experimental results. In sections 3 and 4 we propose models for the theoretical interpretation of NMR spectra of nematic and solid phases, respectively. In section 5 we discuss the results and extract the physical implications of the proposed interpretation. In section 6 we give our conclusions and close this paper with a remark on the expected technological relevance of this investigation.

2. Experimental Results

Synthesis and characterization of the samples used in this work were reported elsewhere.[18] After purification, the samples were introduced into normal NMR glass tubes, degassed, and sealed under vacuum ($\sim 10^{-5}$ torr). This process involved several melting–solidification cycles in the absence of any orienting field. The degassed and solidified

0024-9297/83/2216-0279$01.50/0

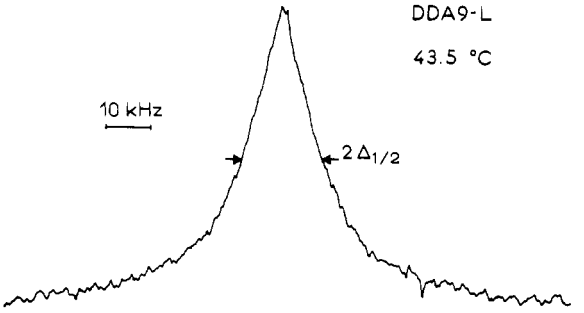

Figure 1. Proton NMR spectrum of DDA9-L in the solid phase at T = 43.5 °C.

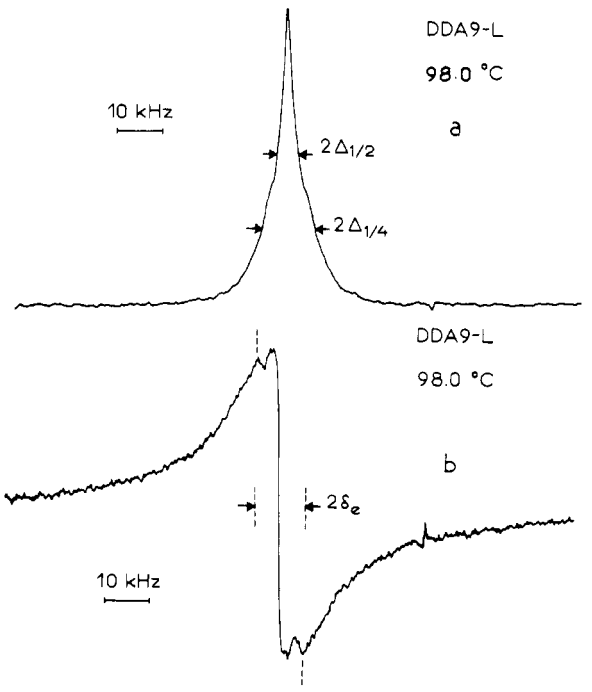

Figure 2. Proton NMR spectra of DDA9-L in the solid phase at T = 98 °C, i.e., one degree below T_{KN}: (a) absorption spectrum; (b) dispersion spectrum.

samples were thereafter introduced into the magnetic field of the NMR spectrometer and the data always recorded at increasing temperature.

The phase transition temperatures listed in Table I were derived from changes in NMR line shapes and line widths, and are in agreement with temperatures measured by means of differential scanning calorimetry.

Proton NMR absorption and dispersion spectra were recorded for the three samples as a function of temperature over their solid, nematic, and isotropic phases, using a Bruker CXP-100 spectrometer working at 49.9 MHz (field strength = 11.7 kG). The temperature of the samples was controlled to within ±0.3 °C with a Bruker B-ST 100/700 temperature-regulating system, and the estimated error in the absolute values was less than 1 °C.

Representative spectra of DDA9-L are shown in Figures 1–3. In Figures 4 and 5 are plotted the line widths of the absorption spectra at quarter- and half-height ($2\Delta_{1/4}$ and $2\Delta_{1/2}$) as a function of temperature for the three samples studied in this work. Note the clear definition of the transition temperatures between thermodynamic phases and the inversion of concavity of the curves $\Delta(T)$ upon passage from the solid to the nematic phase. In the nematic phase of DDA9-L, $2\delta_N$ represents a dipolar line splitting (Figures 3 and 4).

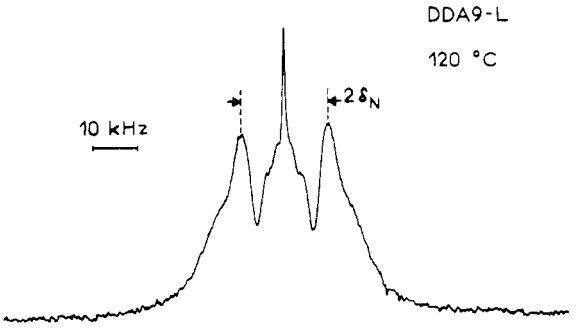

Figure 3. Proton NMR spectrum of DDA9-L in the nematic phase at T = 120 °C. The splitting $2\delta_N$ reflects the strong alignment of the macromolecules in the magnetic field of the spectrometer.

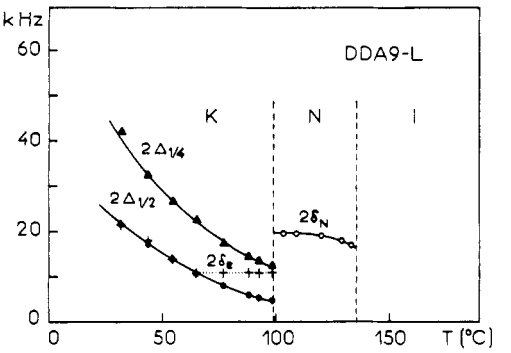

Figure 4. Temperature variations of spectral parameters defined in Figures 1–3 in the solid (K) and nematic (N) phases of DDA9-L.

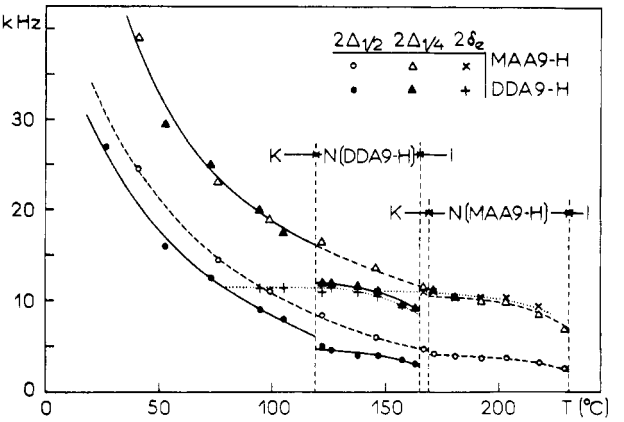

Figure 5. Temperature variations of spectral parameters defined in Figures 1–3 in the solid (K) and nematic (N) phases of DDA9-H and MAA9-H. Note the coincidence of the curves $2\Delta_{1/4}(T)$ in the solid phase of both polymers.

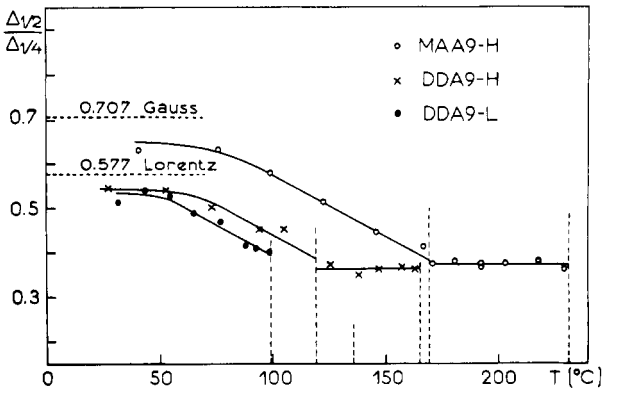

Figure 6. Temperature variation of the ratio $\Delta_{1/2}/\Delta_{1/4}$ in the solid and nematic phases of DDA9-H and MAA9-H and in the solid phase of DDA9-L.

The ratios $\Delta_{1/2}/\Delta_{1/4}$ are plotted in Figure 6. We see that they are constant near room temperature and decrease monotonically with increasing temperature up to the solid–nematic transition T_{KN}. At this temperature there is a discontinuity in $\Delta_{1/2}/\Delta_{1/4}$ and this ratio then remains constant over the temperature range of the nematic phase.

2.1. DDA9-L. Two different absorption line shapes can be observed in the solid phase of this polymer, Figures 1 and 2a. Between room temperature and about 60 °C the spectrum appears as a single broad line (Figure 1) with a "super-Lorentzian" shape, i.e., one in which the wings spread out more than in the true Lorentzian, and consequently the ratio $\Delta_{1/2}/\Delta_{1/4}$ is lower than 0.577, as seen in Figure 6. Above 60 °C and up to the solid–nematic transition point T_{KN}, the line shape changes to the mixed form illustrated in Figure 2a, which appears to be a combination of a broad line with a narrower component in the center. These two components appear more clearly in the dispersion spectrum shown in Figure 2b.

The ratio $\Delta_{1/2}/\Delta_{1/4}$ is about 0.54 between room temperature and ~60 °C and then decreases monotonically with increasing temperature, to reach the value 0.40 at T_{KN} (Figure 6). This nonuniform narrowing of the absorption line results in the appearance above 60 °C of the composite line shape of Figure 2a.

There is a drastic change both in the line shape and in the spectrum width at the solid-to-nematic transition temperature T_{KN}. Above T_{KN} the NMR spectrum appears to be the combination of a symmetric doublet with a central line showing some structure, as illustrated in Figure 3. The separation of the doublet lines, $2\delta_N$, is of dipolar origin and reflects a macroscopic alignment of the polymer in the nematic phase. Note that $2\delta_N \simeq 4\Delta_{1/4}(T_{KN})$. The temperature dependence of $2\delta_N$ is qualitatively similar to the one observed for the order parameter S in low-molecular-weight nematic liquid crystals. The spectrum of DDA9-L is reminiscent of that of nematic PAA[19] but the methyl groups in the 2 and 2′ positions of DDA9, as well as its flexible spacers, give rise to some distinctive spectral features, which will be discussed in section 3.

At the nematic-to-isotropic transition temperature the spectrum collapses to a single narrow line of about 500 Hz, a width arising from the magnetic field inhomogeneity of our spectrometer.

2.2. DDA9-H. In the solid phase the NMR spectra of this polymer show the same qualitative form as in DDA9-L. At the solid–nematic transition there is a discontinuous change in the line width but the line shape remains *qualitatively* the same—in constrast to what is observed with DDA9-L. There is no homogeneous macroscopic alignment (over sample dimensions) in this case, at least not for residence times of the order of 1 h in the magnetic field of 11.7 kG used in this work.

As shown in Figures 5 and 6, the line width behavior as a function of temperature in the solid phase of DDA9-H is similar to that of DDA9-L. The ratio $\Delta_{1/2}/\Delta_{1/4}$ is about 0.54 at room temperature, decreases to 0.39 at T_{KN}, and is 0.36 in the nematic phase.

2.3. MAA9-H. For this polymer we have observed qualitatively the same line shapes and temperature behavior as for DDA9-H, except that the discontinuities of $\Delta_{1/2}$ and $\Delta_{1/4}$ at the solid-to-nematic transitions are much less pronounced (Figure 5).

At room temperature the ratio $\Delta_{1/2}/\Delta_{1/4}$ reaches in this case a value of about 0.65, which is between the Lorentzian and the Gaussian values (0.577 and 0.707, respectively). Its qualitative behavior does not deviate, however, from the preceding ones, as shown in Figure 6: at about 70 °C it starts to decrease monotonically with increasing temperature and reaches a value of about 0.39 at T_{KN} (the same as that found for DDA9-H). In the nematic phase of MAA9-H we have $\Delta_{1/2}/\Delta_{1/4} \simeq 0.38$, which is to be compared with the value 0.36 found for DDA9-H.

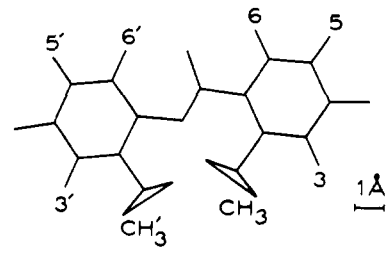

Figure 7. Geometric structure of the mesogenic unit of DDA9 and MAA9 polymers in the planar conformation as inferred from X-ray data on PAA (see text). Note the distorted character of this moiety.

3. Approximate Simulation of the NMR Spectrum of DDA9-L in the Nematic Phase

We have previously mentioned that the proton NMR spectrum of DDA9-L in the nematic phase (Figure 3) is reminiscent of that of nematic PAA.[19] The entire spectrum is symmetric about the resonance frequency and extends over ~50 kHz, and the splitting $2\delta_N$ of the external doublet varies with temperature (Figure 4) in a way similar to that known for the order parameter S of low-molecular-weight nematic liquid crystals.[19,20] These remarks unambiguously suggest that the spectrum is completely dominated by partially averaged out dipolar interactions. Starting from this secure basis, we shall now try to understand the precise shape of the spectrum observed.

The rigorous simulation of the proton NMR spectrum of this polymer is not feasible for two main reasons: the precise geometry of the repeating unit is unknown, and there are too many interacting proton spins in the system without special symmetry. We have, therefore, looked for a semiquantitative solution to this problem under the following approximations:

(a) The geometry of the mesogenic unit has been assumed to be the same as that of PAA,[22] with, of course, the modifications imposed by the presence of methyl groups in the 2 and 2′ positions of the azoxy groups of DDA9. It is pictured to scale in Figure 7, where the two anisole fragments have been drawn coplanar for the sake of clarity; actually the dihedral angle β between them may be rather large.[23] Note also the distorted character of this mesogenic element, which is important in the evaluation of some interproton distances; it was observed in the solid phase of PAA[22] and is apparently preserved in its nematic phase.[19,23]

(b) The complete system of 32 proton spins in the repeating unit of the polymer was divided into several "weakly coupled" subsystems, and in computing the NMR spectrum, we have neglected the coupling between these subsystems.

This method has been shown to produce valuble results in the case of PAA,[19] and has the advantage of being workable with the help of a small desk computer.

3.1. Outline of the Computation. In the present case of DDA9 it is certainly a good first approximation to neglect the interaction between the protons in the aliphatic spacer and those in the mesogenic moiety. For further subdivision into "independent" subsystems of spins, we proceeded as follows. For each of the conformations I and II of the mesogenic moiety, we have allowed for an adjustable dihedral angle β between the benzene planes and

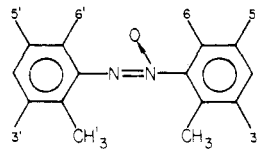

I

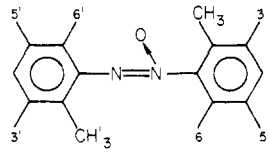

II

considered the following combinations of presumed "independent" spin subsystems:

I.1: (CH_3, CH_3') + (3, 5, 6) + (3′, 5′, 6′) + (spacer)

I.2: (CH_3, CH_3') + (3) + (3′) + (5, 6, 6′, 5′) + (spacer)

I.3: (CH_3, CH_3') + [(3, 5, 6)...(6′, 5′, 3′)] + (spacer)

II.1: (CH_3, 3) + (6, 5) + (CH_3', 3′) + (6′, 5′) + (spacer)

II.2: (CH_3) + (3, 5, 6) + (CH_3') + (3′, 5′, 6′) + (spacer)

The spectrum (line positions and intensities) of each subsystem denoted (···) was then computed by retaining only the Zeeman and dipole–dipole interactions in the corresponding Hamiltonian, in coherence with the introductory remarks in this section. In the case I.3, the notation [(3, 5, 6)...(6′, 5′, 3′)] means that we took an approximate Hamiltonian for this group of six protons consisting of the sum of the Hamiltonian of (3, 5, 6) with the Hamiltonian of (3′, 5′, 6′) plus a perturbative dipolar interaction between protons 6 and 6′, which links these two subgroups of three protons each. The spectrum of the protons in the spacer was estimated in a manner to be described below. Finally, we have simulated the complete NMR spectrum of DDA9-L by adding the theoretical spectra of presumed independent spin subsystems according to each of the five combinations I.1, ..., II.2 specified and performing their convolution with an appropriate line shape function. The intensities of partial spectra were, of course, scaled to the corresponding number of spins, and the width of the line shape function, the nematic order parameter S, and the angle β between the benzene rings were treated as adjustable parameters. The quantities β and S are important outputs of this computation and will be further considered below.

We tried to fit to the experimental spectrum of DDA9-L at 120 °C, Figure 3, every one of the five spectra constructed in this way. The best result was obtained with combination I.3 and is given in Figure 8a, together with the experimental spectrum for comparison. In Figure 8b this simulated spectrum is split up into its mesogenic moiety and spacer contributions. The former was obtained with $S = 0.80$, $\beta \simeq 36°$, and a Gaussian line shape function of width $2\Gamma = 2.4$ kHz at half-height. The latter consists of three Gaussians centered at $\nu_0 = 0$ and $\nu_{1,2} = \pm 12.5$ kHz, with relative intensities 2.7:1:2.7 and widths $2\Gamma_0 = 7.0$ kHz and $2\Gamma_{1,2} = 10$ kHz.

Let us now consider separately the three subsystems entering in I.3, viz., (CH_3, CH_3'), [(3, 5, 6)...(6′, 5′, 3′)], and the protons in the spacer.

3.2. Subsystem (CH_3, CH_3'). In the planar ($\beta = 0$) conformation, Figure 7, the distance between the methyl groups (measured between their centers of gravity) is $d(CH_3,CH_3') \simeq 2.8$ Å. Because of the predominance of dipolar effects in the observed spectrum, as discussed above, we may write the Hamiltonian for this subsystem as follows:

$$\hbar^{-1}\mathcal{H} = \hbar^{-1}(\mathcal{H}_Z + \mathcal{H}_D) = \sum_\alpha \omega_0 I_Z^\alpha + \sum_{\alpha>\beta} D_{\alpha\beta}[I_Z^\alpha I_Z^\beta - \tfrac{1}{4}(I_+^\alpha I_-^\beta + I_-^\alpha I_+^\beta)] \quad (1)$$

where α and β refer to the spins

$$D_{\alpha\beta} = \gamma^2\hbar\langle(3\cos^2\theta_{\alpha\beta} - 1)r_{\alpha\beta}^{-3}\rangle S \quad (2)$$

and

$$S \equiv \tfrac{1}{2}\langle 3\cos^2\theta - 1\rangle \quad (3)$$

is the nematic order parameter; $\theta_{\alpha\beta}$ is the angle made by the proton–proton vector $\mathbf{r}_{\alpha\beta}$ with the long (inertial) axis of the mesogenic unit, θ is the angle made by this axis with the local nematic director, and the other symbols have their usual meaning. The approximations involved in writing eq 1 and 2 are well-known (see, e.g., ref 19 and 23) and will not be repeated here; the errors resulting from these approximations are negligible compared to those produced by neglecting the coupling between the subsystems introduced in 3.1. We can obtain the spectral frequencies and intensities for this subsystem from those given in ref 24 for the A_3A_3' spin system, neglecting the spin–spin coupling ($J = 0$). This spectrum has 34 lines distributed symmetrically about the Larmor frequency $\nu_0 = \omega_0/2\pi$. It is strongly dependent on β, the angle between the benzene rings, and for $\beta = 36°$ and $S = 0.80$ it contributes only to the central part of the experimental spectrum. The most important contributions come around $\nu = \pm 3.5$ kHz and $\nu = 0$.

3.3. Subsystem [(3, 5, 6)...(6′, 5′, 3′)]. In the planar conformation of the benzene rings, the distance $d(6,6') \simeq 4.4$ Å, $d(5,6) = 2.48$ Å, and $d(3,5) = 4.29$ Å. We treated this subsystem as an association of two equivalent groups of spins, viz., (3, 5, 6) and (6′, 5′, 3′), coupled by the perturbative dipolar interaction between spins 6 and 6′. The total Hamiltonian for this subsystem may thus be written

$$\mathcal{H} = \mathcal{H}(3,5,6) + \mathcal{H}(6',5',3') + \mathcal{H}_D'(6,6') \quad (4)$$

where the explicit expressions for the various terms have the structure defined in eq 1–3. The terms $\mathcal{H}(3,5,6)$ and $\mathcal{H}(6',5',3')$ commute and have the same energy levels and equivalent eigenfunctions. So, if ψ_j and E_j are the eigenfunctions and energy levels of the three-spin system,[25] $\psi_{jk} = \psi_j\psi_k$ and $E_{jk} = E_j + E_k$ are the corresponding eigenfunctions and energy levels of the Hamiltonian $\mathcal{H}_0$ given by

$$\mathcal{H}_0(3,5,6;6',5',3') \equiv \mathcal{H}(3,5,6) + \mathcal{H}(6',5',3') \quad (5)$$

This Hamiltonian has 8 nondegenerate states, 22 doubly-degenerate states, and 3 fourfold-degenerate states. The total Hamiltonian

$$\mathcal{H} = \mathcal{H}_0(3,5,6;6',5',3') + \mathcal{H}_D'(6,6') \quad (6)$$

was handled analytically by the usual method of perturbation theory, and after rather long and tedious calculations we found a spectrum of 150 lines distributed symmetrically about ω_0. This result was checked by putting in the final expressions $r_{6,6'} \to \infty$ (see eq 6 and 2): we recovered the initial spectrum of the three-spin system.[25]

This 150-line spectrum is relatively independent of the dihedral angle β between benzene groups, but it is strongly affected by variations in the degree of order S. For $S = 0.80$ the lines concentrate around $\nu = 0$ and $\nu = \pm 9$ kHz.

3.4. Subsystem of Spacer Protons. The spacer unit of DDA9 contains 10 methylene groups. The computation of the NMR spectrum of this subsystem of 20 protons, with time-variable conformation and multiple dipolar interactions, is impossible. However, it is known that short methylene chains either free[26] or linked at one end to the mesogenic units[27] in liquid crystals are constrained[28] to conform, on the average, to a certain orientation imposed by the mean field potential of the liquid crystalline state. In the latter case it is known also that the chains follow the long-wavelength orientational fluctuations of the ne-

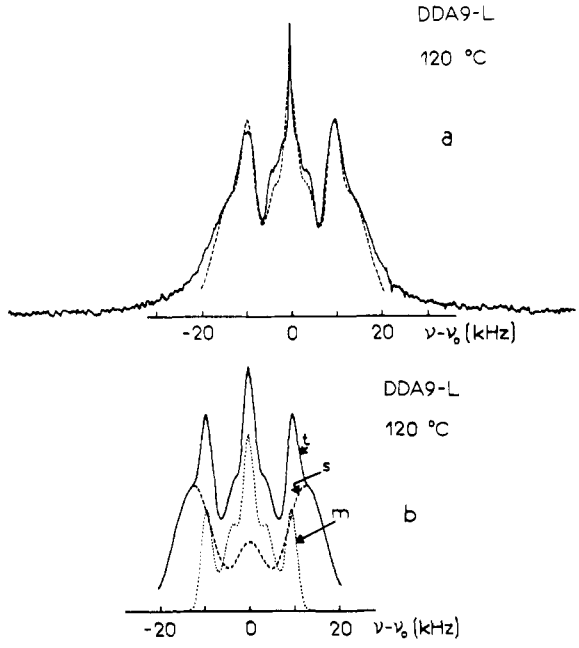

Figure 8. (a) Comparison of simulated (dashed line) and observed proton NMR spectra of DDA9-L in the nematic phase at $T = 120$ °C; (b) decomposition of the simulated spectrum (t) into its mesogenic unit (m) and spacer (s) components.

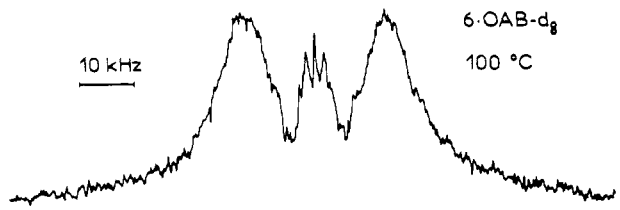

Figure 9. Proton NMR spectrum of 4,4′-bis(hexyloxy)azoxybenzene *deuterated* on the benzene rings (6OAB-d_8): only chain protons are observed. Nematic phase, $T = 100$ °C, $S = 0.82$. The external doublet splitting is about 25.8 kHz.

matic director,[29] which confirms the constrained behavior.[28] The NMR results[27] show that the order along a singly-linked short aliphatic chain is highest at the linkage point and decreases to some "free chain" value with increasing distance to this point. In linear polymers with mesogenic elements connected by short flexible spacers we expect the spacers to be well ordered at the connection points and to show, on the average, lower but not vanishing order in between. Comparison of deuteron NMR results obtained with free[26] and linked chains[27] further suggest that the doubly-linked spacer in DDA9 should be roughly comparable, as far as NMR is concerned, with a singly-linked chain with half-length. So, we assumed in this work that the NMR spectrum of the subsystem of spacer protons under consideration should be qualitatively similar to the corresponding spectrum of the nematic homologue of PAA with five CH_2 groups in the aliphatic chains, i.e., 4,4′-bis(hexyloxy)azoxybenzene *deuterated* on the mesogenic unit (6OAB-d_8).

Figure 9 shows the proton NMR spectrum of 6OAB-d_8 in the nematic phase. The spectrum is symmetric about the resonance frequency and shows essentially three broad lines with roughly Gaussian shapes. The central line is weaker than the external ones and has a small triplet superimposed on it. This small triplet comes from the terminal methyl groups, and the three broad lines are due to the five methylene groups in the chain. The most striking feature of this spectrum is that the splitting of the external lines is given by

$$2\delta\nu = \frac{3}{2\pi}\frac{\gamma^2\hbar}{r^3}|S| \tag{7}$$

where $|S| \simeq S/2$ is the degree of order of an isolated pair of CH_2 protons aligned, on the average, perpendicularly to the long axis of the mesogenic moiety (degree of order S). This situation corresponds to the chain being aligned, on the average, with the mesogenic moiety.

In the case of DDA9 we coherently expected that the apparent (unresolved) NMR spectrum of the subsystem of spacer protons should exhibit three broad, roughly Gaussian, lines, the external ones being centered at $\nu = \pm 12.5$ kHz, which corresponds to $|S| = S/2$ and $S = 0.80$ as found for the other subsystems considered above (the widths and intensities of the three Gaussians were given above). These features were indeed found from the fitting procedure described above and appear in the NMR spectrum of the spacer shown in Figure 8b.

4. NMR Spectra of Unoriented Samples

As noted in section 2 the line shapes of the NMR spectra of DDA9-L, DDA9-H, and MAA9-H in their solid phases near T_{KN}, as well as the line shapes of DDA9-H and MAA9-H in their nematic phases, are *qualitatively* the same (Figure 2). This implies some similarity in the structural organization of all these phases. Indeed, our NMR results, as well as X-ray observations,[21] suggest that all these phases, solid and nematic, may be viewed as built up from a great number of small, roughly homogeneous or "monocrystalline" (solid or liquid) domains randomly oriented in space. This multidomain picture is an *operational concept* that satisfies our purposes here; it will be made precise and further discussed in section 5.2. The domains are certainly *rather soft* in the high-temperature region of the solid phase of these polymers: our results suggest that near their solid–nematic transition points T_{KN}, virtually all motions except the long-range translational motions are practically free, the latter being liberated at the transition itself.

To prove that this view is consistent with our experimental results, let us take the case of DDA9-L in the solid phase near T_{KN}, Figure 2a, and assume that the observed sample was composed of a great numer of small domains, each containing approximately the same number of molecules. To each domain we associate a local director $\mathbf{n}_c$ defining the mean orientation of the macromolecules, or, more precisely, the mean orientation of the ensemble of macromolecular repeating units. The domains are randomly oriented and fixed in the sample space but within each of them we allow for internal rotations and small-amplitude reorientational motions of the long axis of the repeating units. Thus, *within* each domain we may define a degree of order $S_c = {}^1/_2\langle 3\cos^2\theta - 1\rangle_c$ in the same way as in the nematic phase, and we expect $S < S_c \lesssim 1$.

Now the proton NMR spectrum of each domain in the solid phase, $f_{K,S_c}(\alpha,\omega)$, may clearly be computed from the spectrum relative to the oriented nematic phase $f_S(\omega)$ (cf. preceding section) by substituting everywhere in the computation $S_cP_2(\cos\alpha)$ for S and multiplying the widths of all lines by a factor $K(T)$; α is the angle made by the domain director $\mathbf{n}_c$ with the external magnetic field, and the factor K is introduced to account for the different widths of the spectral lines in the solid and nematic phases. We assume, naturally, that at each temperature the values of S_c and K are independent of α and that S_c is the same for all domains. For the spacer contribution to the NMR spectrum of each domain we assume that the area ratio of the central to the external lines of the broad triplet is conserved and that the external lines are now centered at

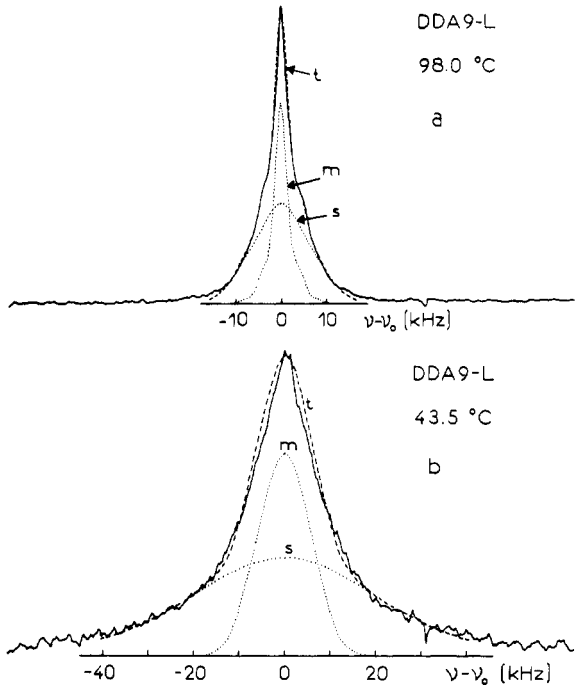

Figure 10. Comparison of simulated (t) and observed proton NMR spectra of DDA9-L in the solid phase: (a) at T = 98 °C, i.e., one degree below T_{KN}; (b) at T = 43.5 °C. Dotted lines represent the mesogenic unit (m) and spacer (s) components of the simulated spectra.

$\nu_c = \pm(12.5/0.8)S_cP_2(\cos\alpha)$ kHz, instead of the value ν = ±12.5 kHz corresponding to the nematic phase with S = 0.80.

The total (observed) spectrum of DDA9-L in the solid phase is then a superposition of the spectra of all domains in the sample and is given by

$$F(\omega) = \frac{1}{4\pi}\int f_{K,S_c}(\alpha,\omega)\,d\Omega \qquad (8)$$

where $d\Omega = \sin\alpha\, d\alpha\, d\phi$ is the elementary solid angle and the integral extends over the unit sphere.

A reasonable approximation of $F(\omega)$ may be obtained by dividing the surface of the unit sphere into 18 bands limited by equally spaced parallels ($\Delta\alpha$ = 10°) and assuming that within each band all domains form the same angle α_n with the external magnetic field, which is along the polar direction of the sphere. This allows the substitution of the integral in eq 8 by a discrete summation:

$$F(\omega) \simeq \frac{1}{4\pi}\sum_{n=0}^{17} f_{K,S_c}(\alpha_n,\omega)\Delta\Omega_n \qquad (9)$$

where $\alpha_n = 10(n + {}^1/_2)$ degrees and

$$\Delta\Omega_n = \int_0^{360} d\phi \int_{10n}^{10(n+1)} \sin\alpha\, d\alpha = 2\pi\{\cos(10n) - \cos[10(n+1)]\} \qquad (10)$$

Taking symmetries into account, we find that only nine directions are relevant and expression 9 simplifies to

$$F(\omega) \simeq \sum_{n=0}^{8} f_{K,S_c}(\alpha_n,\omega)\{\cos(10n) - \cos[10(n+1)]\} \qquad (11)$$

Expression 11 was used to compute the NMR spectrum of DDA9-L in the solid phase, starting from the corresponding spectrum relative to the nematic phase at 120 °C, as given in Figure 5. Satisfactory results were obtained for $S_c \simeq 0.9$ and K = 1.1 at 98 °C and for $S_c \simeq 1$ and K = 5 at 43.5 °C. These results are contrasted to the corresponding experimental spectra in Figure 10. Assuming that $S_c \simeq 1$ for $T \lesssim 65$ °C, we have also obtained the following values, to be used later: K = 3.8 at 54.4 °C and K = 2.5 at 65 °C.

5. Discussion

5.1. Macroscopically Oriented Samples. One striking feature of our results is the macroscopically homogeneous orientation of the macromolecules in the nematic phase of DDA9-L induced by a magnetic field of about 10 kG. This is inferred from the spectrum width and symmetry, which are certainly a consequence of the dominating action of partially averaged out dipolar interactions, and is unambiguously confirmed by the analysis in preceding sections. That this homogeneous orientation is set up at the solid-to-nematic transition temperature is shown by the sudden broadening of the spectrum at this temperature.

The microscopic structure of this ordered phase, as well as its order parameter S, eq 3, may, in principle, be inferred from NMR data with excellent accuracy. In fact, the rigorous interpretation of our data is prevented by the complexity of the spin system and the lack of precise geometrical data on the macromolecules, as stressed in section 3. Considering these dificulties, the simulated spectra shown in Figures 8 and 10 are rather satisfactory approximations of the actual spectra and may be used to extract reliable information.

The simulated spectrum of DDA9-L in the nematic phase at 120 °C reproduces the main features of the experimental spectrum, Figure 8a, namely, the shoulders at ±3.5 kHz on the central portion of the experimental spectrum, the valleys at ±6 kHz, the peaks at ±9.5 kHz, and the shoulders on the external doublet at ±12.5 kHz. Other features such as the long wings of the experimental sepctrum, the sharp peak at the center, and the shoulders at ±1.3 kHz are not reproduced. These differences may be irrelevant for the following reasons. The shoulders at ±1.3 kHz as well as the sharp peak at the center of the experimental spectrum probably come from the end groups of the macromolecules, which we have neglected in the computations described above (section 3). In this respect we remember that the small triplet superimposed on the central line in the spectrum of 6OAB-d_8, Figure 9, is also due to the end-chain CH_3 groups of this material. The outer lines of this small triplet are at ±1.6 kHz from the center, but the chain is shorter in this case (five CH_2 groups) than in the case of DDA9 (ten CH_2 groups), and we know that in liquid crystals the order along a methylene chain linked at one end to the mesogenic unit decreases with increasing distance to the linkage point.[27] One possible explanation for the longer wings of the experimental spectrum could be the distortion introduced by the experimental setup (receiver dead time, etc.), which is difficult to avoid in recording such a wide spectrum. Other factors such as the approximations involved in decoupling the methyl protons from their neighbors in the mesogenic moiety or an appreciable density of orientational defects (disclinations) may also contribute to such details of the experimental spectrum.

Considering the assumptions in section 3 and the satisfactory agreement found between observed and computed spectra shown in Figure 8a, we can safely conclude the following:

(a) The most probable conformation of the mesogenic units in the macromolecule is such that the benzene rings form a dihedral angle of *about* 36° at 120 °C, and the methyl groups stay on the side opposed to the oxygen (configuration I in section 3). The dihedral angle between the benzene planes may depend on temperature, as in PAA.[23]

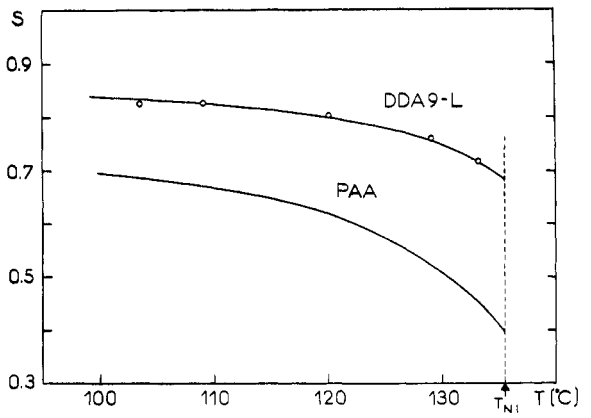

Figure 11. Order parameter S as a function of temperature in the nematic phase of DDA9-L and comparison with PAA. The circles represent experimental points (this work); the curve for PAA was obtained from data in ref 23.

(b) The nematic order parameter S is found to take unusually high values in DDA9-L, as compared with low-molecular-weight liquid crystals. At 120 °C we find $S \simeq 0.80$ and since S is proportional to the splitting $2\delta_N$, Figures 3 and 4, the complete curve $S(T)$ can be established for the nematic phase of this polymer. It is shown in Figure 11, together with the corresponding curve for PAA for comparison. To our knowledge this is the first time that the full curve $S(T)$ is given for the order parameter of a nematic polymer. Approximate values of $S(T_{NI})$ and $S(T_{KN})$ were given by us in a preliminary short communication of this work.[30] Alignment of another thermotropic nematic polymer of the same type (mesogenic unit and flexible spacer in the main chain) was reported[31] but the order parameter, as measured by X-rays, was only given at one temperature.

The value $S(T_{NI}) = 0.69$ found in this work is in perfect agreement with the value $S(T_{NI}) = 0.685$ obtained from magnetic birefringence measurements.[21] From the analysis in section 3 we estimate the error of our values of $S(T)$ to be less than ± 0.05.

It may be interesting to note that this value of $S(T_{NI})$ is closer to that predicted by the Onsager theory of nematic order than to the value predicted by the Maier and Saupe theory.[20] The approach of Onsager was designed for very long rods, i.e., with length to diameter ratio $L/D > 10$, a condition that is fulfilled by the nematic polymers studied here but not by the low-molecular-weight nematics.[32] In fact, the latter are better described by the Maier and Saupe theory.[20] Although it might be tempting to conclude that an Onsager-type theory applies to the nematic state of this kind of macromolecules, more work should be done to firmly establish such a structure–property relationship.

The unusually high values of $S(T)$ may be a consequence of the restriction on orientational fluctuations coming from the mesogenic units being connected by the spacers.

(c) The flexible spacers that connect the mesogenic units of DDA9-L are, on the average, in a rather extended conformation. The corresponding orientational order is comparable to that of the mesogenic units, as we have seen in section 3: a degree of order $S = 0.80$ was required *both* for the mesogenic unit and for the spacer in order that the experimental spectrum could be satisfactorily recovered by the simulated one at 120 °C. Although there certainly exist slight bendings producing misalignments of the polymer chains in the magnetic field, our results suggest that the density of hairpin-bend defects should be rather low in the oriented nematic phase of DDA9-L. We can safely conclude that the average chain conformation is, in this case, a rather extended one. The X-ray diffraction pattern for a nematic glass of DDA9-L obtained by quenching the ordered nematic liquid further supports this model of an extended repeating unit.[33]

5.2. Solid and Nematic Unoriented Samples. Turning now to the results obtained in section 4, we first note the satisfactory agreement between the observed and computed spectra, Figure 10. The main difference between them is the slightly greater width of the upper part of the simulated spectra; this comes from a similar difference in the computed nematic spectrum at 120 °C, Figure 8a, from which we started in section 4, and so it is not meaningful.

It is doubtless that the oriented and unoriented nematic phases have both the same *microscopic* structural organization. They only become different when very long orientational correlations are considered. The concept of a multidomain structure as applied in section 4 to unoriented nematics such as DDA9-H and MAA9-H is not satisfactory, however. More precisely, we certainly were dealing with strongly (and randomly) distorted nematic structures with some density of disclinations[20] rather than with "polycrystalline" nematics. To the purposes developed in section 4 both concepts are equivalent.

In the solid phase between about $T_{KN} - 30$ °C and T_{KN}, the NMR spectra (e.g., Figure 2a) remain very similar in shape to those observed in the unoriented nematic phase, thus suggesting similar microscopic structures. On the other hand, these spectra resemble very much the characteristic spectra observed with conventional semicrystalline polymers such as polyethylene (PE). The latter have been interpreted in terms of three components of different line widths (broad, medium, and narrow) corresponding to the immobile protons of the crystalline, and the "hindered" and "freely" mobile protons of the two kinds of amorphous regions, respectively.[34]

The separation of a broad-line proton NMR spectrum, similar to that shown in Figure 2a, into two or three components corresponding to different proton mobilities, and so to different material structures, is certainly a meaningful method as applied to polymers such as PE, whose repeating unit is simple. In our case, where the repeating units of the polymers are rather complex and formed by two parts of quite different rigidities and where half of the protons of the rigid (mesogenic) moiety (i.e., the methyl protons) are dynamically distinct from the others, a similar decomposition of the NMR spectra would be at least highly controversial. Note that the starting point of our analysis in section 4 was the oriented nematic phase spectrum simulated in section 3, which was also obtained from three components (three independent groups of protons), but with a different meaning.

The main differences between this model and that used for PE[34] are the following:

(a) Our model accounts for different mobilities of the repeating unit of the polymer at different temperatures through the factor $K(T)$ introduced in section 4, including different mobilities of the three main groups of protons in the repeating unit; it does not account for different mobilities of these groups of protons (or the repeating unit) at a given temperature in different regions of the sample.

(b) In our model the material is considered more homogeneous than in the classical fringed-micelle or crystalline–amorphous model. We assume that the main sources of *structural* inhomogeneity are the material defects. We also assume strong *spatial* inhomogeneities due to orientational distortions, in analogy with low-molecular-weight nematics.[20] Note that homogeneity is being considered here at a scale greater than the length of the

polymer repeating unit. From this point of view we should not consider as inhomogeneous a smectic-like lamellar structure resulting from the semirigid character of the polymer repeating unit.

Considering the quality of our results (which could be further improved at the expense of more cumbersome calculations than the simple ones considered in sections 3 and 4) and considering the mesogenic character of our polymers (with the implications of this property at the molecular level), we believe that in the temperature range studied here, these polymers are actually more homogeneous than assumed in the conventional models. Their microscopic structure in the solid phase above ~60° C probably consists of orientationally ordered arrangements of the macromolecules (or their repeating units), with some density of defects (dislocations and disclinations) and bearing a continuous transition from the ordered regions to the dislocations or disclinations. The orientationally ordered regions, which we call "domains" in section 4, may have a frozen nematic-like structure or a lamellar (smectic-like) structure; the latter is suggested by X-rays.[33] Our NMR data are apparently inconclusive on this particular; they suggest, however, that translational diffusion is strongly restricted below T_{KN}. This structure in ordered regions is obtained below T_{KN} even on cooling from the oriented nematic phase, which means that the nematic-to-solid phase transition strongly disturbs the long-range orientation, just as usual in low-molecular-weight nematics.

More detailed and specific structural studies, both by NMR and by other complementary techniques, are required for the complete clarification of the microscopic structure of these polymers. If our simple model proves to be insufficient or inadequate to explain future results and a conventional cystalline–amorphous structure has to be considered for these polymers also (when viewed at a scale greater than the length of the repeating unit), then it will be necessary to reanalyze the NMR spectra into at least six or nine components at our level of approximation (i.e., with three "independent" groups of spins)! Fortunately, some simplifications are possible, e.g., by partially deuterating the polymers or by using ^{13}C NMR.

Above ~60 °C all our samples become soft to some degree, and the NMR spectra are largely insensitive to the relative positions of the macromolecular segments because of various internal motions which set up and are very effective in averaging out intermolecular spin–spin interactions. We can gain insight into the nature of such internal motions from the values of the parameter $K(T)$ introduced in section 4, which is proportional to the elementary width $\Gamma(T)$ of the spectral lines of the NMR spectrum. As $\Gamma(T)$ is proportional to the effective correlation time τ_c of the motions, we may write

$$K(T) \sim \tau_c \sim \exp(W/k_B T) \tag{12}$$

where W is an effective activation energy. From the values taken by K at different temperatures (see the end of section 4), we find

$$W \cong 6.6 \text{ kcal/mol} \tag{13}$$

which equals the value reported for similar motions in the nematic phase of *p*-azoxyanisole.[35] We conclude that in the solid phase of our polymers the decrease of the NMR spectral width (as measured by $\Delta_{1/2}$ or $\Delta_{1/4}$) with increasing temperature is essentially a motional narrowing effect.

On the other hand, in the nematic phase the variation of the spectrum width with temperature is clearly dominated by the order parameter $S(T)$, thus giving rise to an inversion of the concavity of $\Delta_{1/2}(T)$ and $\Delta_{1/4}(T)$ at the solid–nematic transition temperature, Figure 5. The constancy of the ratio $\Delta_{1/2}/\Delta_{1/4}$, as shown in Figure 6, is another proof of that.

A detailed analysis of the NMR spectrum of the mesogenic moiety of DDA9-L in the high-temperature region of the solid phase (labeled m in Figure 10a) reveals that the shoulders that appear in the lower part of the absorption line profile originate in the spin system denoted [(3, 5, 6)...(6′, 5′, 3′)] in section 3. This spin system is responsible for the strong peaks at $\nu - \nu_0 = \pm\delta_N$ of the NMR spectra in the nematic phase (Figures 3 and 8) and for the peaks observed at $\nu - \nu_0 = \pm\delta_e$ in the dispersion spectra of the unoriented samples at higher temperatures (Figures 2b, 4, and 5). Thus, the splitting $2\delta_e$ is an indirect measure of the local order of the mesogenic units and the fact that it is constant in the solid phase near T_{KN} means that the orientational fluctuations of the mesogenic units of our polymers are strongly restricted in this (soft) region.

Our data on the NMR line width behavior with temperature, Figures 5 and 6, show three additional features. First, in spite of the structural and thermodynamic differences between DDA9-H and MAA9-H, the curves $\Delta_{1/4}(T)$ for these two polymers are coincident in their solid phases, but the curves $\Delta_{1/2}(T)$ are not (Figure 5). Second, the plots of the ratio $\Delta_{1/2}/\Delta_{1/4}$ as a function of temperature give parallel straight lines in the upper region of the solid phase of the three polymers studied here (Figure 6). Finally, in contrast to the behavior of both $\Delta_{1/2}$ and $\Delta_{1/4}$, which systematically decrease with increasing temperature over the full range of our measurements, their ratio $\Delta_{1/2}/\Delta_{1/4}$ decreases linearly with increasing temperature just below T_{KN} but is nearly constant about room temperature (Figure 6).

These facts are interrelated and certainly reflect distinct structural and dynamic properties of the two polymer moieties, namely, the (rather rigid) mesogenic unit and the flexible spacer. However, the present data seem to be insufficient to differentiate clearly and quantitatively the behavior of one moiety from the other. New (dynamic) data are required and further work is currently under way. This point is thus left for a future publication.

6. Conclusion

From this preliminary investigation of a new class of thermotropic nematic liquid crystalline polyesters with mesogenic elements and flexible spacers in the main chain, we have been able to disclose some microscopic peculiarities of these materials that may help us to understand various structure–property relationships. An outstanding feature of our results is the homogeneous orientation of the macromolecules in the nematic phase of DDA9–L, with a degree of order significantly higher than those currently reported for other materials. Moreover, it is shown that the flexible spacers take, on the average, an extended conformation with a degree of orientational order comparable to that of the mesogenic moieties.

This result, if confirmed for other systems, is of particular interest. It suggests that highly oriented materials such as perhaps high-strength fibers might be produced from low-melting thermotropic nematic polymers. This would lead to soluble and melt-processible materials without sacrifice of the directional properties hitherto associated only with structures that are based on rigid high-melting repeating units.

Acknowledgment. A.F.M. acknowledges the hospitality of the members of the Equipe de Physico-Chimie Moléculaire, DRF/Ph.S., CENG, where part of his contribution to this work was carried out. R.B.B. and A.B. acknowledge support of their work by the National Science

Foundation under Grant DMR-79-17397.

Registry No. DDA9 (copolymer), 79062-62-7; DDA9 (repeating unit), 79079-27-9; MAA9 (copolymer), 84041-39-4; MAA9 (repeating unit), 79079-25-7; 6OAB-d_8, 84041-40-7.

References and Notes

(1) Kwolek, S. L. U.S. Patent 3 600 350 (Aug 17, 1971); U.S. Patent 3 819 587 (June 25, 1974).
(2) Morgan, P. W. *Macromolecules* **1977**, *10* (6), 1381.
(3) Kuhfuss, H. F.; Jackson, W. J., Jr. U.S. Patent 3 778 410 (Dec 11, 1973); U.S. Patent 3 804 805 (Apr 16, 1974).
(4) Jackson, W. J., Jr.; Kuhfuss, H. F. *J. Polym. Sci., Polym. Chem. Ed.* **1976**, *14*, 2043.
(5) Roviello, A.; Sirigu, A. *J. Polym. Sci., Polym. Lett. Ed.* **1975**, *13*, 455. *Eur. Polym. J.* **1979**, *15*, 61.
(6) Blumstein, A.; Sivaramakrishnan, K. N.; Clough, S. B.; Blumstein, R. B. *Mol. Cryst. Liq. Cryst. (Lett.)* **1979**, *49*, 255. *Polym. Prepr., Am. Chem. Soc., Div. Polym. Chem.* **1978**, *19* (2), 190. *Polymer* **1982**, *23*, 47.
(7) Griffin, A. C.; Havens, S. J. *Mol. Cryst. Liq. Cryst. (Lett.)* **1979**, *49*, 239.
(8) Fayolle, B.; Noel, C.; Billard, J. *J. Phys. (Paris)* **1979**, *40* (C3), 485.
(9) Strzelecki, L.; van Luyen, D. *Eur. Polym. J.* **1980**, *16*, 299.
(10) Millaud, B.; Thierry, A.; Strazielle, C.; Skoulios, A. *Mol. Cryst. Liq. Cryst. (Lett.)* **1979**, *49*, 299.
(11) Jin, J.-I.; Antoun, S.; Ober, C.; Lenz, R. W. *Br. Polym. J.* **1980**, 132.
(12) Antoun, S.; Lenz, R. W.; Jin, J.-I. *J. Polym. Sci., Polym. Chem. Ed.* **1981**, *19*, 1901.
(13) Meurisse, P.; Noel, C.; Monnerie, L.; Fayolle, B. *Br. Polym. J.* **1981**, *13*, 55.
(14) Blumstein, A.; Sivaramakrishnan, K. N.; Vilasagar, S.; Blumstein, R. B.; Clough, S. B. In "Liquid Crystals of One- and Two-Dimensional Order"; Helfrich, W., Heppke, G., Eds.; Springer-Verlag: New York, 1980; p 252. *Prepr., IUPAC Macromol. Sympo. Florence* **1980**, *3*, 298.
(15) Vilasagar, S.; Blumstein, A. *Mol. Cryst. Liq. Cryst. (Lett.)* **1980**, *56*, 263.
(16) van Luyen, D.; Liebert, L.; Strzelecki, L. *Eur. Polym. J.* **1980**, *16*, 307.
(17) Krigbaum, W. R.; Ciferri, A.; Asrar, J.; Toriumi, H. *Mol. Cryst. Liq. Cryst.* **1981**, *76*, 79.
(18) Blumstein, A.; Vilasagar, S. *Mol. Cryst. Liq. Cryst. (Lett.)* **1981**, *72*, 1.
(19) Martins, A. F. *Port. Phys.* **1972**, *8*, 1.
(20) de Gennes, P.-G. "The Physics of Liquid Crystals"; Clarendon Press: Oxford, 1975.
(21) Maret, G.; Volino, F.; Blumstein, R. B.; Martins, A. F.; Blumstein, A. "Proceedings of the 27th IUPAC International Symposium on Macromolecules, Strasbourg, 1981"; Vol II, p 973.
(22) Krigbaum, W. R.; Chatani, Y.; Barber, P. G. *Acta Crystallogr., Sect. B.* **1970**, *B26*, 97.
(23) Volino, F.; Martins, A. F.; Dianoux, A. J. *Mol. Cryst. Liq. Cryst.* **1981**, *66*, 37.
(24) Emsley, J. W.; Lindon, J. C. "NMR Spectroscopy Using Liquid Crystal Solvents"; Pergamon Press: Oxford, 1975; Table 3.9.
(25) Andrew, E. R.; Bersohn, R. *J. Chem. Phys.* **1950**, *18*, 159.
(26) Samulski, E. T. *Ferroelectrics* **1980**, *30*, 83.
(27) See, e.g.: Deloche, B.; Charvolin, J. *J. Phys. (Paris)* **1976**, *37*, 1497. Bos, P. J.; Pirs, J.; Ukleja, P.; Doane, J. W. *Mol. Cryst. Liq. Cryst.* **1977**, *40*, 59.
(28) Martins, A. F. *Phys. Rev. Lett.* **1980**, *44*, 158.
(29) Martins, A. F.; Bonfim, J. B.; Giroud-Godquin, A. M. *Port. Phys.* **1980**, *11*, 159.
(30) Volino, F.; Martins, A. F.; Blumstein, R. B.; Blumstein, A. *Hebd. Seancer C. R. Acad. Sci.* **1981**, *292*, II-829. *J. Phys. (Lett.), Paris* **1981**, *42*, L-305. Note that the molecular weight and the degree of polymerization of DDA9-L were wrongly given in tese references; the correct values are those given in Table I here.
(31) Liebert, L.; Strezlecki, L.; van Luyen, D.; Levelut, A. M. *Eur. Polym. J.* **1981**, *17*, 71.
(32) Stephen, M. J.; Straley, J. P. *Rev. Mod. Phys.* **1971**, *46*, 617.
(33) Blumstein, A.; Vilasagar, S.; Ponrathnam, S.; Clough, S. B.; Maret, G.; Blumstein, R. B. *J. Polym. Sci., Polym. Phys. Ed.* **1982**, *20*, 877.
(34) Bergmann, K. *J. Polym. Sci., Polym. Phys. Ed.* **1978**, *16*, 1611.
(35) Schwartz, M.; Fagerness, P. E.; Wang, C. H.; Grant, D. M. *J. Chem. Phys.* **1974**, *60*, 5066.

Kerr Effect and Dielectric Study of Poly(vinyl chloride) and Its Oligomers

Garo Khanarian, Frederic C. Schilling, Rudolf E. Cais, and Alan E. Tonelli*

Bell Laboratories, Murray Hill, New Jersey 07974. *Received May 12, 1982*

ABSTRACT: We present experimental results for the molar Kerr constant ${}_mK$ and mean square dipole moment $\langle\mu^2\rangle$ for the two isomers of 2,4-dichloropentane (meso (m) and racemic (r)), the three isomers of 2,4,6-trichloroheptane (mm, mr, and rr), and poly(vinyl chloride) (PVC). We calculate configurational averages of ${}_mK$, $\langle\mu^2\rangle$, and $\langle\gamma^2\rangle$ (mean anisotropy squared) for these molecules using the rotational isomeric state model of Williams, Pickles, and Flory. We find a strong sensitivity of ${}_mK$ and $\langle\mu^2\rangle$ to the first-order parameter E_η, which accounts for chlorine–methine carbon interactions, and to the second-order parameter $E_{\omega''}$, which accounts for chlorine–chlorine atom interactions. We find that E_η and $E_{\omega''}$ are significantly less attractive and more repulsive, respectively, than deduced by Flory and co-workers. Deviations of bond rotational positions from 0° and ±120° are of the order of 3°. PVC stereoregularity or tacticity has a strong influence on ${}_mK$ and $\langle\mu^2\rangle$, particularly in the highly isotactic and syndiotactic regions. We find fair agreement between the calculated and observed values of ${}_mK$, $\langle\mu^2\rangle$, and $\langle\gamma^2\rangle$ for PVC and its oligomers.

Vinyl polymers $-CH_2(CHRCH_2)_xCHR-$ differ from other long-chain molecules in two important respects.[1] The substitution of an R group for an H atom at every other carbon atom in polymethylene tends to severely restrict the allowed backbone conformations about a pair of successive rotatable bonds due to steric overlap and coulombic repulsion. Also, since alternate carbons are asymmetrically substituted, the characteristics of the chain will depend sensitively on the stereochemical composition of such centers of asymmetry. This has been demonstrated experimentally and theoretically for several configurational properties of vinyl polymers, viz., end-to-end distance,[2] NMR chemical shifts,[3] dipole moments,[4] depolarized Rayleigh scattering,[5] and Kerr effect.[6-9] The chain property last mentioned, i.e., the Kerr effect, appears to be one of the most sensitive to the configurational properties of flexible polymers as demonstrated recently by calculation[6,7] and experiment.[6,8,9]

In this paper we utilize the Kerr effect and dipole moments to characterize poly(vinyl chloride) (PVC) and its oligomers 2,4-dichloropentane (DCP) and 2,4,6-trichloroheptane (TCH). We present experimental values of the molar Kerr constant ${}_mK$ and dipole moment squared $\langle\mu^2\rangle$ and also their calculated values, based on a rotational

0024-9297/83/2216-0287$01.50/0